



Innovative Complex Coacervates of Gelatin and Sodium Carboxymethyl Cellulose for Cinnamaldehyde Delivery: Impact of Processing Conditions on Characteristics and Bioactivity

Mahran Abdulla^{1,2}, Shuqin Xia^{1,*}

¹School of Food Science and Technology, Collaborative Innovation Center of Food Safety and Quality Control, Jiangnan University, 1800 Lihu Road, Wuxi, Jiangsu 214122, P. R. China

²Food Science Department, Faculty of Agriculture, Cairo University, 12613 Giza, Egypt

* Corresponding author

Received: 30 Oct 2023; Received in revised form: 02 Dec 2023; Accepted: 10 Dec 2023; Available online: 31 Dec 2023

©2023 The Author(s). Published by Infogain Publication. This is an open access article under the CC BY license

(<https://creativecommons.org/licenses/by/4.0/>).

Abstract— Cinnamaldehyde (CA) has a special flavor, and numerous bioactivities; nevertheless, it possesses a high level of volatility, low solubility in water, and limited stability. To address the shortcomings of CA and enhance its use in foods, CA-loaded microcapsules were created by complex coacervation. Gelatin (GL) and carboxymethyl cellulose (CMC) were used as the wall materials of CA. Ideal conditions for obtaining encapsulation efficiency and morphology were found for core/wall ratio 1:1 (w: w), and an emulsification speed 15,000 rpm. The optimized microcapsule formulation demonstrates an encapsulation efficacy of 87.949 ± 1.229 % for CA with payload 41.276 ± 4.189 % and a size of 26.093 ± 0.575 µm. The examination of Fourier-transform infrared (FTIR) spectra of GL, CMC, GL-CMC complex coacervates and CA microcapsules exhibited an electrostatic attraction among GL and CMC molecules and the creation of hydrogen bonds among core (CA) and shell materials. When 1:1 core: wall ratio and 9000 rpm emulsification speed utilized in the microencapsulation of CA, the thermal stability significantly enhanced, possessed a slow-release property in ethanol 50%, and enhanced the antibacterial activity of CA.

Keywords— Complex coacervates, Cinnamaldehyde, Core/wall ratio, Emulsification, Encapsulation efficiency, Antimicrobial activity, Release properties.

I. INTRODUCTION

Cinnamaldehyde (CA), the primary compound found in cinnamon oil obtained from cinnamon bark, is an aromatic aldehyde with low water solubility and has received approval from the Joint FAO/WHO Expert Committee on Food Additives (JECFA) for its use as a potential food-flavoring agent [1,2]. Furthermore, CA possesses garnered increased attention because of its inherent properties such as antibacterial, anticancer, antioxidant, insecticidal, and anti-inflammatory effects [3]. Despite these positives, there are significant challenges associated with its direct application, including low solubility in water, high volatility, susceptibility to harsh environmental conditions

(e.g., high temperatures, elevated ionic strength, and extreme pH), interaction with active components, and the potential to introduce an undesirable flavor that may impact the overall taste of foods [3,4]. To address these issues, various encapsulation methods have been explored to enhance its solubility in water and regulate its volatility, preserve its flavor, and enable sustained release over an extended period.

Microencapsulation involves enclosing various food components within a tiny protective shell or coating to safeguard them and enable their gradual release. This technology is extensively utilized to enhance the application of CA, which faces limitations. Among the

various techniques available, complex coacervation-based microencapsulation stands out due to its substantial capacity for loading, effective sustained release, and resistance to high temperatures, all achieved under mild conditions [5,6]. Complex coacervation hinges on the electrostatic attraction among biopolymers with opposite charges [7]. The formation of coacervates necessitates careful control of several process parameters, including pH, temperature, ionic strength, stirring speed, biopolymer ratios, molecular weight, and biopolymer concentration [8]. Typically, complex coacervation is performed using positively charged proteins and anionic polysaccharides.

Gelatin (GL) and sodium carboxymethyl cellulose (CMC) are two organic, safe, and environmentally degradable biopolymers that readily dissolve in water, extensively utilized in the pharmaceutical and food sectors [9]. GL, sourced from collagen, possesses excellent gelling, film-forming, and emulsifying properties. CMC, a cellulose derivative created by partially substituting cellulose hydroxyl groups at positions 2, 3, and 6 with carboxymethyl [10], is more commonly used due to its favorable qualities, including biocompatibility, biodegradability, and cost-effectiveness [11]. A study conducted by J. Zhang et al. [12], provided valuable insights and contribute to the creation of microcapsules via complex coacervation employing GL and CMC. These microcapsules have the potential to safeguard bioactive compounds that are sensitive to heat, as well as flavors and food ingredients such as zeaxanthin. Another study by Duhoranimana et al. [13], demonstrated that GL-CMC complex coacervates have the ability to be employed in microencapsulation, safeguard and transport bioactive components and food ingredients that are sensitive to heat. This study also highlighted the function of pH and the mixing ratio of GL to CMC in complex coacervation. Nevertheless, it was noted that high ionic strength and variations in pH can diminish or totally disrupt the electrostatic attraction among GL and CMC, affecting the rheological characteristics of the coacervates [14]. In complex coacervation, it is imperative to optimize the process to produce particles with desired characteristics. Factors such as emulsification speed and the core: wall ratio of microcapsules prepared through complex coacervation are pivotal, as they impact the ultimate attributes of microcapsules, including encapsulation efficiency, particle size, shape, and agglomeration rate [15]. These characteristics, in turn, influence release properties and antimicrobial effectiveness. Hence, this present study aims to investigate how processing conditions, such as emulsification speed and core: wall ratio, influence microcapsule size, shape, encapsulation efficiency, release properties, and antimicrobial activity.

Additionally, the study delves into the thermal stability of CA microcapsules through thermogravimetric analysis.

II. MATERIALS AND METHODS

2.1. Materials

Gelatin (GL) (BLV 225, type B, isoelectric point ranging from 4.70 to 5.20) was sourced from Chengdu Classic Gelatin Co., Ltd. in Sichuan, China. FL9 Sodium carboxymethyl cellulose (CMC) (with a viscosity of 20.0 mPa s and a degree of substitution of 1) was acquired from Yixing Tongda Chemical Co., Ltd. in Jiangsu, China. Cinnamaldehyde (CA) (98%) was procured from Ji'an Jupeng Natural Flavor Oil Co., Ltd. located in Jilin, China. Hexane and Pure Ethanol Absolute were obtained from Sinopharm Chemical Reagent Co., Ltd. in Shanghai, China. Deionized water (Milli-Q) was employed in the preparation of all aqueous solutions.

2.2. Preparation of biopolymer solution

Solutions of GL/CMC were prepared at a predetermined mass concentration of 1% by weight. The procedure involved dissolving a specific quantity of GL and CMC in a 9:1 ratio in deionized water. This dissolution process took place with gentle stirring in a bath of water maintained at a temperature of 60°C for a period of 2 hours [16].

2.3. Preparation of cinnamaldehyde microcapsules

Microcapsules containing CA were created using a GL/CMC mixture with a ratio of 9:1 (w/w). CA was introduced into the previously prepared solution, where the wall material concentration was set at 1% (weight/volume). This was done while varying the core/wall ratios (1:1 and 2:1, w/w). Subsequently, the mixture was subjected to high-speed dispersion using a device that ran for 2 minutes at different speeds: 9000, 12000, and 15000 revolutions per minute (r/min). Following the emulsification step, the solutions were stirred gently at a temperature of 45°C for a duration of 30 minutes, maintaining an optimal pH of 4.5 with the addition of acetic acid at concentrations of 10%, 1%, and 0.1%, v/v. Afterward, the solution was cooled down using an ice bath. Once the temperature dropped below 15°C, it was maintained for 0.5 hours while stirring at a rate of 400 revolutions per minute (r/m) [17]. The subsequent steps involved allowing the system to settle overnight at 6°C, subsequently centrifugation at 2000 rpm for 4 minutes. The resulting material was then frozen and underwent the process of freeze-drying at 55 ± 7 bar, with the condenser temperature maintained at -78°C, over a period of 48 hours using a Scientz-18N freeze dryer (Ningbo Scientz

Biotechnology Co. Ltd, China). The resulting CA microcapsule powder was stored in a desiccator.

2.4. Morphology of suspension and dried microcapsules

Microcapsule suspensions were examined for their morphology under optical microscopy (BX51, Olympus Corporation, Japan) at a 50× magnification. To study the morphology of the dried microcapsules, a scanning electron microscope (SU8100, JEOL Ltd., Tokyo, Japan) was used. This analysis was performed at a voltage acceleration of 3 kV, and various magnifications were employed. For the scanning electron microscope examination, the microcapsules were initially evenly attached to a specimen holder through the application of double-sided tapes and subsequently applying a thin gold coating [18].

2.5. Particle size

For the determination of the particle size of CA loaded microcapsules before the drying process, a laser particle size analyzer (S3500, Microtrac Inc., USA) was employed. This analyzer was equipped with a sample tank designed for liquid dispersion. Ultrapure water with a pH of 7.0 served as the testing medium [19,20].

2.6. Determination of encapsulation efficiency, and payload

The determination of both free CA and total CA content was carried out in accordance with the method described by Liu et al. [21], using the organic solvent extraction technique. In this process, 0.1 gram of CA microcapsules were dispersed in a 10 mL n-hexane solution. To extract the surface oil, the mixture was oscillated for 30 seconds at ambient temperature and then allowed to settle. The amount of surface oil was determined by measuring the supernatant absorbance at 285 nm. The calibration curve for CA had a linear range of 0.0–8.0 µg/mL, with the standard curve represented by $y = 0.165x - 0.0205$ ($R^2 = 0.9992$), where y is the CA absorbance at 285 nm, and x is the free CA concentration in µg/mL. For the determination of total oil content, 0.1 grams of microcapsules were added to a 70 mL absolute ethanol solution and subjected to sonication (40°C, 20 kHz, 600 W) for 40 minutes, followed by centrifugation at $12,000 \times g$ for 15 minutes at 25°C. The gathered precipitate underwent three washes with an ethanol solution, and the resulting supernatants from both stages were utilized to determine the total oil amount at 285 nm, following a linear range of CA from 0.0–8.0 µg/mL, with a measured standard curve of $y = 0.1229x - 0.002$ ($R^2 = 0.9992$), where y is the absorbance of CA at 285 nm, and x is the concentration (µg/mL) of free CA. The encapsulation efficiency and payload of microcapsules were computed by equations (1) and (2), respectively.

$$EE(\%) = (X1 - Xs) / X1 \times 100 \quad (1)$$

$$PL(\%) = X1 / X_m \times 100 \quad (2)$$

In these equations, X1 represents the total weight (g) of CA in the microcapsules, X2 is the mass (g) of CA initially loaded in the system, Xs is the mass (g) of oil on the surface of the microcapsules, and X_m corresponds to the weight of dried CA microcapsules.

2.7. Thermal gravimetric analysis (TGA)

Thermal gravimetric analysis was conducted employing a thermal gravimetric analyzer (TGA/SDTA851e, Mettler-Toledo Corporation, Switzerland). Samples, including the coacervates, free CA and microcapsules each weighing 3–5 mg, were carefully measured on the TGA microbalance. They were then subjected to heating at a rate of 20°C per minute, ranging from 25 to 500°C. Nitrogen gas, flowing at a rate of 20 ml per minute, served as the heating medium. This analysis was conducted to assess the thermal characteristics of the sample powders [3].

2.8. Fourier transform infrared spectroscopy (FTIR)

The FTIR (Fourier-transform infrared) spectra of various materials, including free CA, GL, CMC, complex coacervates, and dried microcapsules, were obtained at ambient temperature (25°C). This analysis was conducted using a Nicolet iS10 FTIR spectrophotometer from Thermo Electron Corp. in Madison, WI. The spectra were collected over a wavenumber range from 400 to 4000 cm⁻¹ with a resolution of 4 cm⁻¹, and the total scan time for each sample was 32 scans. The samples were blended with potassium bromide (KBr) at a ratio (1:100). The resulting mixture was ground and then pressed onto a ZnSe plate. The sample spectrum was acquired with air spectrum subtraction. These procedures were in accordance with the methodology outlined by Q. Liu et al. [22].

2.9. Determination of release properties

The release properties of CA in a 50% ethanol solution were conducted following the methodology described by Bustos C et al. [23], albeit with some adjustments. In this modified procedure, 10 mg of microcapsules or 4.3 mg of free CA were placed within a dialysis bag (cut off 14000 daltons, Sinopharm, Shanghai, China), and these bags were subsequently immersed in 100 ml of a solution consisting of 50% ethanol and 50% water. This 50% ethanol solution is a recognized standard simulant, referred to as simulant D2, utilized for migration studies as per CREU [24]. The samples were placed in an orbital shaking incubator, maintaining a temperature of 25°C and an agitation rate of 20 revolutions per minute in a dark environment throughout the entire testing duration. At predetermined time intervals, the absorbance of the solutions was assessed at 285 nm. After each

measurement, the samples were returned to the system to maintain consistent conditions throughout the experiment. The cumulative release of CA was calculated using equation (3).

$$\text{Cumulative release (\%)} = R1/R2 \times 100 \quad (3)$$

in this equation, R1 and R2 depict the masses of released CA and encapsulated CA, respectively.

2.10. Determination of antimicrobial ability

To investigate the antimicrobial properties of free and encapsulated CA, two common microbial strains, namely *Escherichia coli* (E. coli) and *Staphylococcus aureus* (S. aureus), were selected. These microbial strains were initially activated by being cultured overnight in Muller Hinton broth using an incubator set at 37°C. Subsequently, they were diluted to reach the colony count equivalent to a standardized inoculum (0.5 Mac-Farland) as per the methodology outlined by S. Zhang et al. [24] with some slight modifications. For the antimicrobial tests, CA, or CA microcapsules, along with 200 µL of the microbial suspension, were introduced into the cone-shaped flasks containing 100 mL of sterilized Muller Hinton broth. In these experiments, the concentration of CA employed was 0.02 mg/mL. Control samples were generated by adding 200 µL of microbial suspension into 100 mL of sterilized Muller Hinton broth in a separate cone-shaped flask. All the cone-shaped flasks were sealed using plastic film and positioned in a stable-temperature incubation shaker operating at 150 rpm and maintained at 37°C. The turbidity of each experimental group was measured at 600 nm every 2 hours to assess the growth condition of the bacteria under examination.

2.11. Statistical analysis

The findings are presented as the mean value ± standard deviation and were analyzed using one-way ANOVA. Statistical significance among mean values was evaluated using Duncan's multiple range tests with a confidence level of 95%. ($p < 0.05$) using SPSS 26.0 software (SPSS Inc., Chicago, IL, USA).

III. RESULTS AND DISCUSSION

3.1. Morphology and particle size of microcapsules

When the unit surface area was kept constant, the spherical shape exhibited a comparatively larger volume, providing increased capacity for encapsulating the core substance. Consequently, the spherical form was preferred in the process of microcapsule preparation. Optical microscopic images and particle size data, as shown in Fig. 1, indicated that all the microcapsules possessed a spherical shape. Lower emulsification speed promoted clustering and the

creation of larger multinuclear capsules, while higher homogenization speeds notably reduced the mean particle diameter and the extent of aggregation. This reduction can be attributed to the shearing force's capacity to break larger droplets into smaller ones and prevent collisions, as previous study [25,26]. Furthermore, an increase in the core-to-wall ratio led to a gradual increase in the mean particle size. This was because a greater quantity of CA became entrapped within the microcapsules, causing more mononuclear microcapsules to collide and accumulate into larger multinuclear microcapsules [27,28].

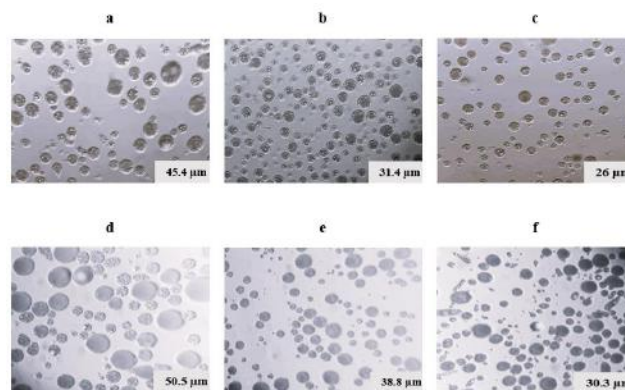


Fig. 1: Morphology of microcapsule suspensions (a, 9000 and 1:1; b, 12000 and 1:1; c, 15000 and 1:1; d, 9000 and 2:1; e, 12000 and 2:1; f, 15000 and 2:1).

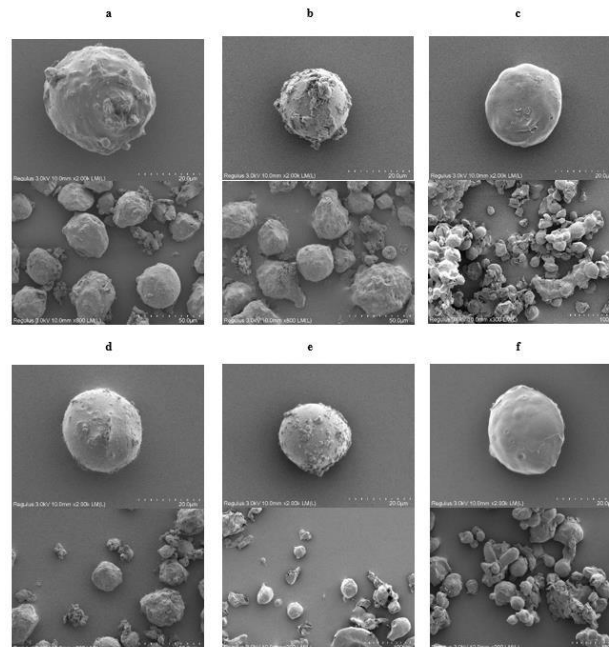


Fig. 2: Electron micrographs of dried microcapsules (a, 9000 and 1:1; b, 12000 and 1:1; c, 15000 and 1:1; d, 9000 and 2:1; e, 12000 and 2:1; f, 15000 and 2:1).

The microstructure of CA-loaded microcapsules was assessed using a scanning electron microscope (Fig. 2).

The images of the microcapsule particles illustrated the influence of homogenization speed on the microstructure and surface properties of the particles. As shown in Fig. 2a, 2b, 2d and 2e the microcapsules are almost spherical shape with rough and compact surface and some aggregation. However, as shown in Fig. 2c and 2f, Microcapsules created at an emulsification speed of 15,000 rpm exhibited a spherical shape with a compact and smoother surface, a higher degree aggregation. A compact wall structure was advantageous for enhancing the barrier properties of the CA-loaded microcapsules, ensuring effective protection and retention of CA. It's worth noting that a study conducted by Muhoza et al. [29], found that freeze-drying could significantly disrupt the microstructure of multinuclear microcapsules.

3.2. Efficacy of Cinnamaldehyde microcapsules Encapsulation and payload

The results pertaining to the efficiency of encapsulation (EE) and payload (PL) of CA microcapsules, which were created using the GL-CMC complex coacervate as a wall material, are summarized in Table 1. Our findings demonstrated that the highest EE and PL were achieved at higher emulsification speeds, it's important to note that elevated emulsification pressures generate emulsions with smaller droplet sizes and create new interfaces, which can lead to re-coalescence and an "over-processing" effect, as observed in the study by Jafari et al. [30]. Similar results were observed in a study by Esfahani et al. [31], where smaller particles and increased particle agglomeration were observed with higher emulsification speeds during the microencapsulation of fish oil, resulting in enhanced encapsulation efficiency. As indicated in Table 1, when the core-to-wall ratio rose from 1:1 to 2:1, there was a reduction in encapsulation efficiency. This reduction can be ascribed to the insufficient availability of wall materials to fully coat the entire core. Consequently, a higher concentration of unencapsulated core material remained, leading to losses during the encapsulation process. This finding aligns with the previous study [32,33].

Table 1. Encapsulation Efficiency, payload, and Particle size of Cinnamaldehyde microcapsules.

Sample	Encapsulation efficiency (%)	Payload (%)	Particle size (μm)
M1	86.166 \pm 0.361 ^b	37.444 \pm 0.978 ^c	45.414 \pm 0.903 ^b
M2	87.036 \pm 0.327 ^{ab}	38.929 \pm 0.982 ^{bc}	31.463 \pm 2.581 ^d
M3	87.949 \pm	41.276 \pm	26.093 \pm

	1.229 ^a	4.189 ^{ab}	0.575 ^e
M4	79.314 \pm 0.565 ^d	33.435 \pm 0.913 ^d	50.492 \pm 1.875 ^a
M5	84.115 \pm 0.324 ^c	43.556 \pm 0.889 ^a	38.863 \pm 3.51 ^c
M6	83.457 \pm 0.543 ^c	41.721 \pm 1.368 ^{ab}	30.381 \pm 0.411 ^d

M1: emulsification speed at 9000 and core-to-wall ratio 1:1, M2: emulsification speed at 12000 and core-to-wall ratio 1:1, M3: emulsification speed at 15000 and core-to-wall ratio 1:1, M4: emulsification speed at 9000 and core-to-wall ratio 2:1, M5: emulsification speed at 12000 and core-to-wall ratio 2:1, M6: emulsification speed at 15000 and core-to-wall ratio 2:1.

3.3. Thermal stability of CA and CA microcapsules

Analysis of thermal stability was carried out on CA, GL-CMC coacervates, and CA microcapsules, spanning a temperature range from 25 to 500°C, aiming to assess the heat resistance of both CA microcapsules and the GL-CMC complex coacervate matrix. The thermogravimetric (TGA) and differential thermogravimetric (DTG) profiles for CA, GL-CMC coacervates, and CA microcapsules are illustrated in Fig. 3. TGA data indicated that free CA experienced a mass loss of 3.3% at 100°C, primarily due to CA volatilization and water evaporation. At 195°C, both TGA and DTG curves exhibited a pronounced weight loss, reaching approximately 89%. A sharp weight mass loss of 89% occurred at 195 °C, indicating rapid volatilization of CA, with only 4.5% of its weight remaining at 500 °C. On the contrary, the GL-CMC complex coacervates displayed a more gradual weight loss, maintaining about 30% of their weight until 500°C, and a DTG minimum was noted at 334°C. This suggests that the shell materials demonstrated resistance to heat and displayed remarkable sustained release characteristics, as reported by Duhoranimana et al. [13]. Comparatively, the stability of microcapsules with core-to-wall ratios of 1:1 and 2:1 (w/w) was considerably greater than that of free CA. Additionally, the graph suggests that an increased core-to-wall ratio resulted in an elevated rate of thermal weight reduction at the same temperature, implying reduced embedding stability. This might be linked to the impact of the core-to-wall ratio on the formation of tight hydrogen bonds between the coacervates and core material, as discussed by Yu et al. [34]. Moreover, microcapsules created at an emulsification speed of 9,000 rpm with a core-to-wall ratio of 1:1 exhibited superior stability compared to other microcapsules, possibly due to the presence of large multinuclear capsules with thick

interfacial membranes, contributing to the stability of the core material and sustained release [35].

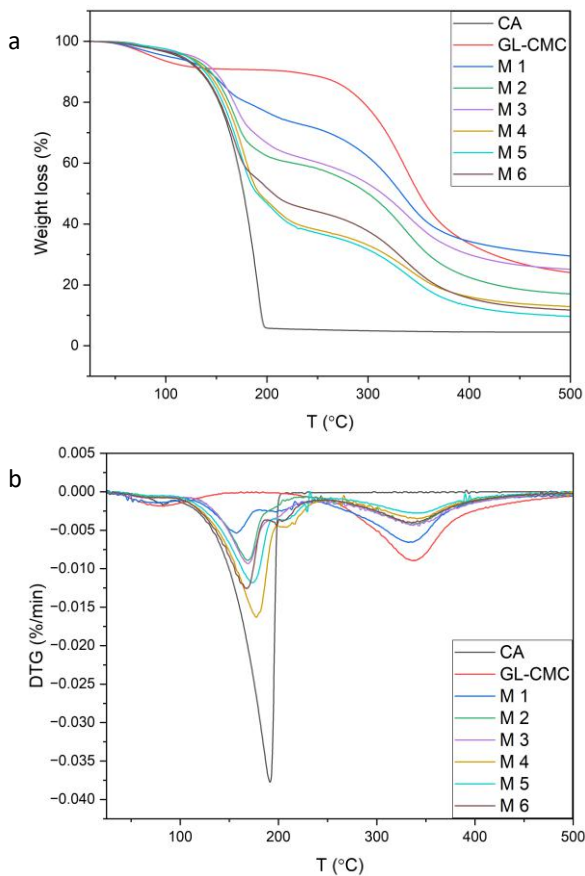


Fig. 3: The TGA (a) and DTG (b) curves of CA, GL-CMC coacervates and CA loaded microcapsules between the temperatures of 25 °C–500 °C.

The combined analysis of TGA and DTG curves demonstrated that the thermal breakdown of different microcapsules could be segmented into three stages. In the first stage, from 25 to 100°C, slight variations occurred, primarily because of water evaporation, resulting in a weight loss of approximately 5%. The second stage, around 200 °C, demonstrated a weight loss of 23%, 37%, 36%, 52%, 53%, and 50%, respectively, for the CA microcapsules. This was significantly higher compared to the almost flat thermal decomposition curve of the GL-CMC complex coacervate at this stage, indicating the liberation of surface core material and a portion of the internal core material. At 350°C, the weight loss increased to approximately 56%, 67%, 62%, 77%, 79%, and 76%, respectively, signifying further core material release. The third stage, from 350 to 500°C, showed a mass loss of 13% for the CA microcapsules, during which the microcapsule mass loss curve aligned with the complex coacervate mass loss curve, indicating the nearly complete evaporation of CA at this stage. Subsequently, this stage primarily

involved the breakdown of the wall substances, in accordance with previous report [36]. Our results were consistent with a research investigation on the microencapsulation of CA, where pectin and GL coacervates were employed [3].

3.4. FTIR features of GL/CMC coacervates and cinnamaldehyde microcapsules.

FTIR analysis was employed to investigate the interaction occurring between the wall materials (GL and CMC) and the core material. The FTIR spectra of GL, CMC, coacervates consisting of GL/CMC, and CA-loaded microcapsules are depicted in Fig. 4. In the FTIR spectrum of GL, a prominent peak was evident at 3436 cm^{-1} , indicative of Hydrogen bonds formed within a molecule manifested as elongation oscillations of N–H bonds ($\nu\text{N-H}$). A secondary peak at 2960 cm^{-1} corresponded to the asymmetric stretching vibrations of C–H bonds ($\nu\text{C-H}$) [37]. Notably, the amide bands displayed three distinct peaks. The peak observed at 1640 cm^{-1} corresponded to the elongation vibrations of the carbonyl group ($\nu\text{C-O}$) within the amide I structure [12]. At 1542 cm^{-1} , a peak denoted the flexing oscillations of the N–H bond ($\delta\text{N-H}$) in amide II, encompassing vibrations of –NH–R bonds at higher wavenumbers and –NH₃ bonds at lower wavenumbers. A weaker peak 1236 cm^{-1} denoted the bending modes of the C–N bond ($\delta\text{C-N}$) of amide III [38]. Furthermore, an intense absorption peak around 1450 cm^{-1} suggested the presence of cis configuration in peptide bonds, likely due to proline or its hydroxylated form, hydroxyproline, within GL, in contrast to the trans configuration found in the majority of protein structures.

In the FTIR spectrum of CMC, a prominent peak at 3432 cm^{-1} was identified, associated with intramolecular hydrogen bonding ($\nu\text{O-H}$) within the cellulose structure. The secondary peak at 2919 cm^{-1} was indicative of the methylene group in CMC. Prominent peaks at 1626 cm^{-1} and 1423 cm^{-1} were assigned to the symmetrical and asymmetrical elongation oscillations of ionized –COO– groups ($\nu\text{-COO-}$), respectively [39]. Furthermore, a robust absorption at 1328 cm^{-1} signified the flexing oscillations of –CH₃ bonds, and the peak at 1057 cm^{-1} was associated with the elongation vibrations of C–O bonds ($\nu\text{C-O}$) [38]. The FTIR spectra obtained from the GL-CMC complex coacervates were essentially a combination of the spectra of pure GL and CMC, with certain absorption peaks shifted positions. A shift towards higher wavenumbers, from 1542 cm^{-1} to 1548 cm^{-1} , indicated the disappearance of the –NH₃ vibration peak at the lower wavenumber. This shift left only the –NH–R vibration peak. Concurrently, the disappearance of the absorption peaks observed at 1626 cm^{-1} and 1423 cm^{-1} , which are associated with the elongation vibrations of –COO– groups in CMC. These

shifts in absorption peaks supported the notion of electrostatic interaction occurring between the $-NH_3^+$ bond of GL and the $-COO^-$ bond of CMC in the process of GL-CMC complex coacervate formation. Importantly, apart from electrostatic interactions, no additional chemical bonds participated in the process of GL-CMC complex coacervate formation, consistent with the findings of Azadirachta et al. [40]. Furthermore, the peaks associated with stretching vibrations of $-OH$ and $N-H$ in the GL-CMC complex coacervates transitioned from 3432 cm^{-1} and 3436 cm^{-1} to 3424 cm^{-1} , respectively. potentially due to alterations in conformation and weak intermolecular interactions among the molecules of GL and CMC, aligning with findings by Lii et al. [41]. The $C-H$ stretching vibration peaks also transitioned from 2960 cm^{-1} and 2919 cm^{-1} to 2941 cm^{-1} , suggesting alterations in conformation occurring between GL and CMC molecules in the process of complex coacervate formation. The spectra of CA-loaded microcapsules exhibited remarkable spectral shifts, reflecting the interaction between CA and the shell materials. Fresh peaks with elevated intensity emerged at 1680 cm^{-1} and 1620 cm^{-1} , characteristic of $C=O$ and aromatic vibrations in CA [42]. These findings are consistent with previous research on the characterization of CA-loaded microcapsules prepared with pectin and GL complex coacervates [3].

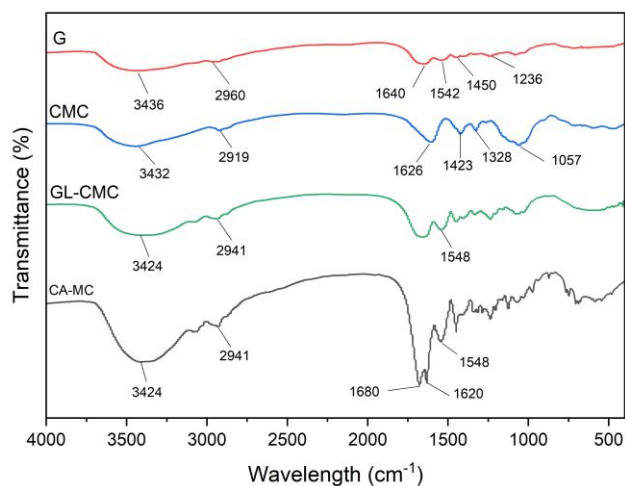


Fig. 4: FTIR spectra of G, CMC and GL-CMC and CA-Microcapsules (CA-MC).

3.5. release properties

The study investigated the release pattern of CA from microcapsule in a 50% ethanol solution simulating food conditions, aiming to assess the stability of these microcapsules within food matrix. The release patterns, depicted in Fig. 5. The dissolution profiles of free CA demonstrated a swift release, reaching 70.8% within 10

minutes and peaking at 82% within 20 minutes. In contrast, the cumulative release curves for CA microcapsules exhibited a notably slower rate of increase. Initially, a swift release (17-28%) occurred within the first 10 minutes, attributed to the surface-absorbed CA and void-released content [43], Subsequently, encapsulated CA within the microcapsules exhibited a gradual release, reaching maximum cumulative release (60-80%) around 150 minutes. Elevating the core-to-wall ratio from 1:1 to 2:1 heightened the cumulative release rate, indicative of reduced protective effects of the wall membrane due to enhanced loading capacity of microcapsules [44]. Consistent with (Khatibi et al. [45], our study observed that an elevated core: wall ratio led to increased cumulative release, akin to the behavior of *Zataria multiflora* Boiss essential oil. Additionally, augmenting homogenization speed amplified the cumulative release rate, in line with the findings of Huang et al. [46], who revealed that Larger multinuclear capsules exhibited enhanced CA retention due to a thicker interfacial membrane. Conversely, microcapsules with a smaller mean particle size exhibited notably lower retention rates. Briefly, microcapsules produced with a core-to-wall ratio of 1:1 and an emulsification speed of 9000 rpm exhibited a lower cumulative release of 60%.

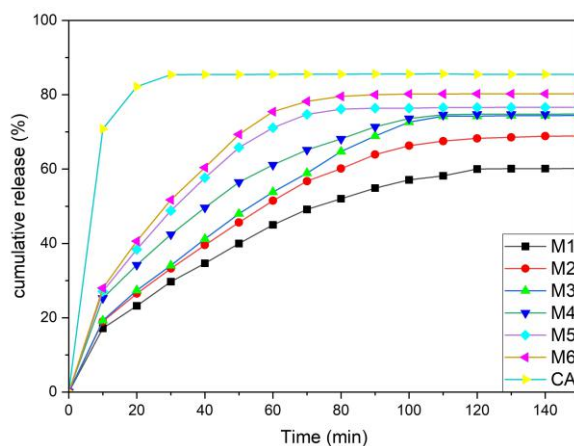


Fig. 5: Release profile of free and microencapsulated cinnamaldehyde in ethanol 50%.

3.6. The antibacterial activity

The antibacterial efficacy of both free CA and CA encapsulated within microcapsules was assessed through the examination of growth curves for the tested bacteria. Fig. 6a illustrates the growth phases (lag, exponential, and stabilization) of *S. aureus*. It was observed that the growth of *S. aureus* in both free and encapsulated CA was more constrained in comparison to the nutrient broth (control) throughout all phases, confirming the antibacterial efficacy of CA against *S. aureus* [47]. The growth rate of *S. aureus*

in encapsulated CA, particularly in microcapsule with a low release profile (M1), was slower than in free CA, suggesting a more robust antibacterial efficacy of encapsulated CA against *S. aureus*. This enhanced effect was attributed to the delayed-release property and improved dispersion of CA facilitated by microcapsules in water, thereby enhancing its efficacy in constraining the metabolism and growth of bacterial cells [48]. As time progresses, the growth curves of free and encapsulated CA gradually aligned, probably because the ongoing erosion of the microcapsule structure diminishes the slow-release characteristic and dispersion capability, thereby diminishing the antibacterial effectiveness of encapsulated CA. The growth curve of *E. coli* mirrored that of *S. aureus* (Fig. 6b). Notably, both free and encapsulated CA demonstrated greater effectiveness in inhibiting *E. coli* compared to *S. aureus*. It's worth noting that gram-positive bacteria, such as *S. aureus*, typically possess a thicker outer cell wall, which may contribute to higher resistance. In contrast, gram-negative bacteria like *E. coli* lack a thick cell wall, this structural distinction may suggest lower resistance in gram-negative bacteria to antibacterial agents [49]. The outcomes presented above underscored the potent antibacterial capability of CA, further augmented through microencapsulation.

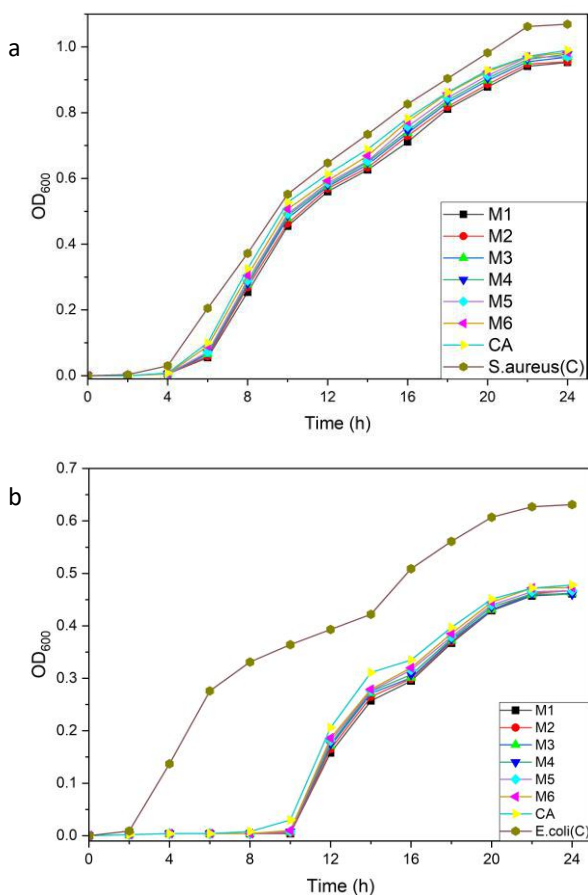


Fig. 6. The antibacterial efficacy of free and encapsulated cinnamaldehyde against *S. aureus* (a) and *E. coli* (b).

IV. CONCLUSION

To address the shortcomings of CA, such as limited stability and low solubility in water, in this study, GL and CMC complex coacervates were used as novel shell materials to microencapsulate CA. The CA-loaded complexes achieved optimal encapsulation efficiency (87.949 ± 1.229 %), morphology and particle size (26.093 ± 0.575 μm) with a core-to-wall ratio of 1:1, and emulsification speed of 15,000 rpm. The CA-loaded microcapsules had greater resistance to heat compared to free CA. The GL-CMC complex coacervate, as outer layer material, enhanced the sustained-release characteristics of CA. The antibacterial efficacy of CA was enhanced after encapsulation. This study offers valuable insights for formulating an optimal microcapsule carrier capable of delivering cinnamaldehyde and various flavors with considerable potential for applications in the food industry by using complex coacervates of CMC and gelatin under different processing conditions.

ACKNOWLEDGEMENTS

The authors greatly appreciate the joint support for study by the program of "Collaborative innovation center of food safety and quality control in Jiangsu Province".

REFERENCES

- [1] E. Chen, S. Wu, D. J. McClements, B. Li, and Y. Li, "Influence of pH and cinnamaldehyde on the physical stability and lipolysis of whey protein isolate-stabilized emulsions," *Food Hydrocoll.*, vol. 69, pp. 103–110, 2017.
- [2] L. Lei, Z. He, H. Chen, D. J. McClements, B. Li, and Y. Li, "Microstructural, rheological, and antibacterial properties of cross-linked chitosan emulgels," *Rsc Adv.*, vol. 5, no. 121, pp. 100114–100122, 2015.
- [3] B. Muhoza, S. Xia, J. Cai, X. Zhang, E. Duhoranimana, and J. Su, "Gelatin and pectin complex coacervates as carriers for cinnamaldehyde: Effect of pectin esterification degree on coacervate formation, and enhanced thermal stability," *Food Hydrocoll.*, vol. 87, no. August 2018, pp. 712–722, 2019, doi: 10.1016/j.foodhyd.2018.08.051.
- [4] Y. Tian, Y. Zhu, M. Bashari, X. Hu, X. Xu, and Z. Jin, "Identification and releasing characteristics of high-amylose corn starch–cinnamaldehyde inclusion complex prepared using ultrasound treatment," *Carbohydr. Polym.*, vol. 91, no. 2, pp. 586–589, 2013.
- [5] Y. Lv, F. Yang, X. Li, X. Zhang, and S. Abbas, "Formation of heat-resistant nanocapsules of jasmine essential oil via gelatin/gum arabic based complex coacervation," *Food*

- Hydrocoll.*, vol. 35, pp. 305–314, 2014.
- [6] A. S. Prata and C. R. F. Grosso, “Production of microparticles with gelatin and chitosan,” *Carbohydr. Polym.*, vol. 116, pp. 292–299, 2015.
- [7] N. Devi, M. Sarmah, B. Khatun, and T. K. Maji, “Encapsulation of active ingredients in polysaccharide–protein complex coacervates,” *Adv. Colloid Interface Sci.*, vol. 239, pp. 136–145, 2017.
- [8] De Kruijff et al., “Complex coacervation of proteins and anionic polysaccharides,” *Curr. Opin. Colloid Interface Sci.*, vol. 9, no. 5, pp. 340–349, 2004.
- [9] Hazirah et al., “Effect of xanthan gum on the physical and mechanical properties of gelatin-carboxymethyl cellulose film blends,” *Food Packag. Shelf Life*, vol. 9, pp. 55–63, 2016.
- [10] Tong et al., “Preparation and properties of pullulan–alginate–carboxymethylcellulose blend films,” *Food Res. Int.*, vol. 41, no. 10, pp. 1007–1014, 2008.
- [11] Carpineti et al., “ β -Lactoglobulin–carboxymethylcellulose core–shell microparticles: Construction, characterization and isolation,” *J. Food Eng.*, vol. 131, pp. 65–74, 2014.
- [12] J. Zhang et al., “Nanoencapsulation of zeaxanthin extracted from *Lycium barbarum* L. by complex coacervation with gelatin and CMC,” *Food Hydrocoll.*, vol. 112, no. December 2019, p. 106280, 2021, doi: 10.1016/j.foodhyd.2020.106280.
- [13] E. Duhoranimana et al., “Effect of sodium carboxymethyl cellulose on complex coacervates formation with gelatin: Coacervates characterization, stabilization and formation mechanism,” *Food Hydrocoll.*, vol. 69, pp. 111–120, 2017, doi: 10.1016/j.foodhyd.2017.01.035.
- [14] Muhoza et al., “Gelatin and high methyl pectin coacervates crosslinked with tannic acid: The characterization, rheological properties, and application for peppermint oil microencapsulation,” *Food Hydrocoll.*, vol. 97, no. June, p. 105174, 2019, doi: 10.1016/j.foodhyd.2019.105174.
- [15] J. C. Roy, S. Giraud, A. Ferri, R. Mossotti, J. Guan, and F. Salaün, “Influence of process parameters on microcapsule formation from chitosan—Type B gelatin complex coacervates,” *Carbohydr. Polym.*, vol. 198, pp. 281–293, 2018.
- [16] Liu et al., “Fabrication of low environment-sensitive nanoparticles for cinnamaldehyde encapsulation by heat-induced gelation method,” *Food Hydrocoll.*, vol. 105, no. February, p. 105789, 2020, doi: 10.1016/j.foodhyd.2020.105789.
- [17] E. Duhoranimana et al., “Thermodynamic characterization of Gelatin–Sodium carboxymethyl cellulose complex coacervation encapsulating Conjugated Linoleic Acid (CLA),” *Food Hydrocoll.*, vol. 80, pp. 149–159, 2018, doi: 10.1016/j.foodhyd.2018.02.011.
- [18] Xu et al., “Effect of Ultrasound Immersion Freezing on the Quality Attributes and Water Distributions of Wrapped Red Radish,” 2015, doi: 10.1007/s11947-015-1496-x.
- [19] L. Qiu, M. Zhang, B. Bhandari, Z. Fang, and Y. Liu, “Size reduction of raw material powder: The key factor to affect the properties of wasabi (*Eutrema yunnanense*) paste,” *Adv. Powder Technol.*, vol. 30, no. 8, pp. 1544–1550, 2019.
- [20] G. Wu, M. Zhang, Y. Wang, K. J. Mothibe, and W. Chen, “Production of silver carp bone powder using superfine grinding technology: Suitable production parameters and its properties,” *J. Food Eng.*, vol. 109, no. 4, pp. 730–735, 2012.
- [21] Liu et al., “Int J of Food Sci Tech - 2022 - Liu - Tannic acid modulated the wall compactness of cinnamaldehyde-loaded microcapsules and.pdf,” *Int. J. Food Sci. Technol.*, 2022.
- [22] Q. Liu et al., “Food Hydrocolloids Fabrication of low environment-sensitive nanoparticles for cinnamaldehyde encapsulation by heat-induced gelation method,” *Food Hydrocoll.*, vol. 105, no. October 2019, p. 105789, 2020, doi: 10.1016/j.foodhyd.2020.105789.
- [23] R. O. Bustos C, F. V. Alberti R, and S. B. Matiacevich, “Edible antimicrobial films based on microencapsulated lemongrass oil,” *J. Food Sci. Technol.*, vol. 53, no. 1, pp. 832–839, 2016, doi: 10.1007/s13197-015-2027-5.
- [24] S. Zhang, M. Zhang, Z. Fang, and Y. Liu, “Preparation and characterization of blended cloves/cinnamon essential oil nanoemulsions,” *LWT*, vol. 75, pp. 316–322, 2017, doi: https://doi.org/10.1016/j.lwt.2016.08.046.
- [25] T. Feng, C. Fan, X. Wang, X. Wang, S. Xia, and Q. Huang, “Food-grade Pickering emulsions and high internal phase Pickering emulsions encapsulating cinnamaldehyde based on pea protein-pectin-EGCG complexes for extrusion 3D printing,” *Food Hydrocoll.*, vol. 124, no. PA, p. 107265, 2022, doi: 10.1016/j.foodhyd.2021.107265.
- [26] Y. Liu and J. Jiang, “Preparation of β -ionone microcapsules by gelatin/pectin complex coacervation,” *Carbohydr. Polym.*, vol. 312, p. 120839, 2023, doi: https://doi.org/10.1016/j.carbpol.2023.120839.
- [27] Z. J. Dong, A. Touré, C. S. Jia, X. M. Zhang, and S. Y. Xu, “Effect of processing parameters on the formation of spherical multinuclear microcapsules encapsulating peppermint oil by coacervation,” *J. Microencapsul.*, vol. 24, no. 7, pp. 634–646, 2007, doi: 10.1080/02652040701500632.
- [28] S. Karagonlu, G. Başal, F. Ozyıldız, and A. Uzel, “Preparation of Thyme Oil Loaded Microcapsules for Textile Applications,” *Int. J. New Technol. Res.*, vol. 4, no. 3, 2018.
- [29] B. Muhoza, S. Xia, X. Wang, and X. Zhang, “The protection effect of trehalose on the multinuclear microcapsules based on gelatin and high methyl pectin coacervate during freeze-drying,” *Food Hydrocoll.*, vol. 105, no. December 2019, p. 105807, 2020, doi: 10.1016/j.foodhyd.2020.105807.
- [30] S. M. Jafari, E. Assadpoor, Y. He, and B. Bhandari, “Re-coalescence of emulsion droplets during high-energy emulsification,” *Food Hydrocoll.*, vol. 22, no. 7, pp. 1191–1202, 2008, doi: https://doi.org/10.1016/j.foodhyd.2007.09.006.

- [31] R. Esfahani, S. M. Jafari, A. Jafarpour, and D. Dehnad, "Loading of fish oil into nanocarriers prepared through gelatin-gum Arabic complexation," *Food Hydrocoll.*, vol. 90, no. December 2018, pp. 291–298, 2019, doi: 10.1016/j.foodhyd.2018.12.044.
- [32] Bastos et al., "core reference.pdf," 2020.
- [33] Y. P. Timilsena, R. Adhikari, C. J. Barrow, and B. Adhikari, "Microencapsulation of chia seed oil using chia seed protein isolate-chia seed gum complex coacervates," *Int. J. Biol. Macromol.*, vol. 91, pp. 347–357, 2016, doi: <https://doi.org/10.1016/j.ijbiomac.2016.05.058>.
- [34] J. Yu, Z. Jingjing, Z. Hongfei, and Z. Bolin, "Microencapsulation of *Elaeagnus mollis* oil to enhance the oxidation stability of polyunsaturated fatty acids: the interaction between fatty acids and wall materials," *Ital. J. Food Sci.*, vol. 32, no. 1, 2020.
- [35] Prata et al., "Influence of the oil phase on the microencapsulation by complex coacervation," *J. Am. Oil Chem. Soc.*, vol. 92, pp. 1063–1072, 2015.
- [36] T. Su, Q.-X. Wu, Y. Chen, J. Zhao, X.-D. Cheng, and J. Chen, "Fabrication of the polyphosphates patched cellulose sulfate-chitosan hydrochloride microcapsules and as vehicles for sustained drug release," *Int. J. Pharm.*, vol. 555, pp. 291–302, 2019, doi: <https://doi.org/10.1016/j.ijpharm.2018.11.058>.
- [37] E. Duhoranimana et al., "Effect of sodium carboxymethyl cellulose on complex coacervates formation with gelatin: Coacervates characterization, stabilization and formation mechanism," *Food Hydrocoll.*, vol. 69, pp. 111–120, 2017, doi: <https://doi.org/10.1016/j.foodhyd.2017.01.035>.
- [38] M. A. S. P. Nur Hazirah, M. I. N. Isa, and N. M. Sarbon, "Effect of xanthan gum on the physical and mechanical properties of gelatin-carboxymethyl cellulose film blends," *Food Packag. Shelf Life*, vol. 9, pp. 55–63, 2016, doi: <https://doi.org/10.1016/j.fpsl.2016.05.008>.
- [39] Singh et al., "Carboxymethyl cellulose-gelatin-silica nanohybrid: An efficient carrier matrix for alpha amylase," *Int. J. Biol. Macromol.*, vol. 67, pp. 439–445, 2014, doi: <https://doi.org/10.1016/j.ijbiomac.2014.03.051>.
- [40] N. Azadirachta, J. Seed, and O. Nso, "Study of Complex Coacervation of Gelatin A with Sodium Carboxymethyl Cellulose : Study of Complex Coacervation of Gelatin A with Sodium Carboxymethyl Cellulose : Microencapsulation of Neem (*Azadirachta indica* A . Juss .) Seed Oil (NSO)," vol. 4037, 2011, doi: 10.1080/00914037.2011.553851.
- [41] C. Lii, P. Tomasik, H. Zaleska, S. Liaw, and V. M.-F. Lai, "Carboxymethyl cellulose-gelatin complexes," *Carbohydr. Polym.*, vol. 50, no. 1, pp. 19–26, 2002.
- [42] B. Muhoza, S. Xia, J. Cai, X. Zhang, E. Duhoranimana, and J. Su, "Gelatin and pectin complex coacervates as carriers for cinnamaldehyde: Effect of pectin esterification degree on coacervate formation, and enhanced thermal stability," *Food Hydrocoll.*, vol. 87, pp. 712–722, 2019.
- [43] Faisant et al., "Release (1).Pdf." 2003.
- [44] M. A. Bayomi, S. A. Al-Suwayeh, A. M. El-Helw, and A. F. Mesnad, "Preparation of casein-chitosan microspheres containing diltiazem hydrochloride by an aqueous coacervation technique," *Pharm. Acta Helv.*, vol. 73, no. 4, pp. 187–192, 1998.
- [45] S. A. Khatibi, A. Ehsani, M. Nemati, and A. Javadi, "Microencapsulation of *Zataria multiflora* Boiss. essential oil by complex coacervation using gelatin and gum arabic: Characterization, release profile, antimicrobial and antioxidant activities," *J. Food Process. Preserv.*, vol. 45, no. 10, 2021, doi: 10.1111/jfpp.15823.
- [46] Y. Huang, B. Sun, and B. Muhoza, "Influence of processing conditions on the physical properties, retention rate, and antimicrobial activity of cinnamaldehyde loaded in gelatin/pectin complex coacervates," *Food Biophys.*, vol. 17, no. 3, pp. 289–301, 2022, doi: 10.1007/s11483-022-09718-x.
- [47] Y. Zhang, X. Liu, Y. Wang, P. Jiang, and S. Y. Quek, "Antibacterial activity and mechanism of cinnamon essential oil against *Escherichia coli* and *Staphylococcus aureus*," *Food Control*, vol. 59, pp. 282–289, 2016, doi: 10.1016/j.foodcont.2015.05.032.
- [48] Y. Sun, M. Zhang, B. Bhandari, and B. Bai, "Nanoemulsion-based edible coatings loaded with fennel essential oil/cinnamaldehyde: Characterization, antimicrobial property and advantages in pork meat patties application," *Food Control*, vol. 127, p. 108151, 2021, doi: <https://doi.org/10.1016/j.foodcont.2021.108151>.
- [49] T. J. Silhavy, D. Kahne, and S. Walker, "The Bacterial Cell Envelope1 T. J. Silhavy, D. Kahne and S. Walker, .," *Cold Spring Harb Perspect Biol*, vol. 2, pp. 1–16, 2010, [Online]. Available: <https://www.ncbi.nlm.nih.gov/pmc/articles/PMC2857177/pdf/cshperspect-PRK-a000414.pdf>